AGU100 ADVANCING EARTH AND SPACE SCIENCE

Earth and Space Science

RESEARCH ARTICLE
10.1029/2019EA000727

A Global/Regional Integrated Model System-Chemistry Climate Model: 1. Simulation Characteristics

Yong-Cheol Jeong[1], Sang-Wook Yeh[1], Seungun Lee[2], and Rokjin J. Park[2]

[1]Department of Marine Science and Convergent Technology, Hanyang University, Ansan, South Korea, [2]School of Earth and Environmental Sciences, Seoul National University, Seoul, South Korea

Key Points:

- We described the simulation characteristics of a newly developed Global/Regional Integrated Model system-Chemistry Climate Model (GRIMs-CCM)
- The GRIMs-CCM simulated the climatological atmospheric features as well as atmospheric teleconnections resulting from tropical SST forcing
- The physical processes that cause biases in the GRIMs-CCM provide further guidance to improve other climate-chemistry models in the CCMI

Correspondence to:
S.-W. Yeh,
swyeh@hanyang.ac.kr

Citation:
Jeong, Y.-C., Yeh, S.-W., Lee, S., & Park, R. J. (2019). A global/regional integrated model system-chemistry climate model: 1. Simulation characteristics. *Earth and Space Science*, *6*, 2016–2030. https://doi.org/10.1029/2019EA000727

Received 27 MAY 2019
Accepted 11 SEP 2019
Accepted article online 14 OCT 2019
Published online 31 OCT 2019

Abstract This study describes the simulation characteristics of a newly developed Global/Regional Integrated Model system-Chemistry Climate Model (GRIMs-CCM), which is listed in Chemistry Climate Model Initiative as a participating model. The GRIMs-CCM was run using a standard set of forcings, and historical sea surface temperatures and sea ice concentration from the Hadley Centre were prescribed. The simulation results of GRIMs-CCM were compared to the National Center for Environmental Prediction/National Center for Atmospheric Research (NCEP/NCAR) reanalysis data set 1. The GRIMs-CCM satisfactorily simulated the climatological (1960–2010) atmospheric features and atmospheric teleconnections resulting from tropical sea surface temperature forcing. However, the GRIMs-CCM also had some regional biases; for instance, particularly, the temperature bias over the Antarctic was noticeable. We further analyzed physical processes that caused such biases and the influence of coupled chemistry-climate processes in the GRIMs-CCM, which may provide further guidance to improve an earlier version of the GRIMs-CCM and other climate-chemistry models participating in the Chemistry Climate Model Initiative.

1. Introduction

It is important to understand the effects of chemicals and aerosols in the atmosphere on the present climate and future climate change (Charlson et al., 1992; Kiehl & Briegleb, 1993; Kim et al., 2016; Ramanathan et al., 2001; Satheesh & Ramanathan, 2000; Yeh et al., 2017). These effects arise from multiple combinations of processes involving aerosols and gaseous chemicals (Haywood & Boucher, 2000; Jeong et al., 2018; Jeong & Park, 2017; Lau et al., 2006). Understanding these complex mechanisms is required to correctly project a future climate. To understand direct and indirect effects of each chemical species, Chemistry Climate Models (CCMs) are necessary. Until now, there are a number of previous studies that have used various CCMs to investigate the interactions between atmospheric chemical components and climate. For example, Kim et al. (2016) found that the anthropogenic sulfate aerosol forcing acts to strengthen the East Asian summer monsoon in recent decades using Community Atmosphere Model version 5 coupled with the modal aerosol model. Zhao et al. (2018) also showed the effects of El Niño and Southern Oscillation (ENSO) on the air pollution in China during winter using CCM in National Climate Center.

Because of such importance of CCMs in chemistry-climate community, the Chemistry Climate Model Initiative (CCMI) was established. The object of the CCMI is to improve the understanding of the chemistry-climate interactions in the Earth system in the past, the present, and in future projections (http://blogs.reading.ac.uk/ccmi/). The CCMI suggested various CCM simulation protocols and recommended CCMI-participating models following them to reduce an uncertainty in understanding of the chemistry-climate interactions. By comparing with various CCM simulations, chemistry-climate community is able to identify and correct unrecognized CCM errors (Eyring et al., 2013). So far, 24 CCMs from various institutes have been listed in CCMI-participating models (http://blogs.reading.ac.uk/ccmi/participating-models/).

In the line of efforts to develop CCMs, a Global/Regional Integrated Model system-Chemistry Climate Model (GRIMs-CCM), which is listed in CCMI-participating models (http://blogs.reading.ac.uk/ccmi/participating-models/), is newly developed. The GRIMs is an Atmospheric General Circulation Model that was created for numerical weather prediction (Hong et al., 2013) and has been applied for various studies, such as for mesoscale (Jang & Hong, 2014; Koo & Hong, 2014) and climate (Chang et al., 2013; Ham et al., 2014; Kim et al., 2014; Lee et al., 2014, 2015; Lee & Hong, 2014). The configuration and evaluation of GRIMs are well

Table 1
GRIMs-CCM Physics Package Used in This Study

Physical parameterization	Scheme	Reference
Convective parameterization scheme	Revised simplified Arakawa-Schubert	Han and Pan (2011)
Microphysical scheme	Weather Research Forecast Single-moment microphysics (WSM3)	Hong et al. (2004)
Land surface	NOAH	Chen and Dudhia (2001) and Ek et al. (2003)
Long wave and short wave radiation	Rapid radiative transfer model for GCMs	Iacono et al. (2008) and Mlawer et al. (1997)
Planetary boundary layer	Yonsei University scheme	Hong et al. (2006)
Gravity wave drag	Orographic flow-blocking drag	Kim and Doyle (2005)
Explicitly coupled shallow convection and planetary boundary layer processes	GRIMs scheme	-

described in Hong et al. (2013). GRIMs reasonably reproduces tropical precipitation patterns including the main rain belt along the Intertropical Convergence Zone comparable to observations (Hong et al., 2013). Similarly, Chang et al. (2013) compared the boreal summer precipitation simulated in GRIMs with the reanalysis data set and they showed that GRIMs was able to reproduce the main characteristics of precipitation variability in East Asia, although GRIMs underestimates precipitation amount over northeast Asia. Furthermore, atmospheric features downscaled by GRIMs accurately reproduced seasonally averaged precipitation and near-surface temperature in East Asia during 1980–2005 (Lee et al., 2014), although a wet bias in precipitation and regional cold and warm biases in temperature were apparent compared to the observations. However, the study on the chemistry-climate interactions has not been studied because of a lack of coupling between chemistry and climate modeling components in GRIMs.

The International Global Atmosphere Chemistry (IGAC) and Stratosphere-troposphere Processes And their Role in Climate (SPARC) communities defined the new CCMI reference (REF) and sensitivity (SEN) simulations (Eyring et al., 2013) for CCM experiments. There are three choices available in REF simulations, REF-C1, REF-C1SD, and REF-C2, respectively (Eyring et al., 2013). The REF-C1 simulation is the reference simulation, which covers the period from 1960 to 2010 with 10 years (1950–1959) of spin-up. The purpose of this simulation is to identify model variability and to reproduce the climate state in the past (1960–2010) when ozone and other atmospheric gases were measured (Eyring et al., 2013). All forcings of this hindcast simulation were based on the observations, that is, empirical data. It includes atmospheric greenhouse gas (GHG) concentrations, anthropogenic and natural emissions of GHGs, including volcanic eruptions, solar irradiance, sea surface temperature (SST), and sea ice concentrations (SIC). In this study, we examined the performance of the GRIMs-CCM to reproduce the historical climate variability under CCMI REF-C1 and examined GRIMs-CCM's internal biases. Analyses of internal biases will help to improve the future performance of chemistry-climate models participating in CCMI.

In section 2 we provide a brief description of GRIMs-CCM and describe the model experiment and reference reanalysis data used during the examination stage. In section 3, the results of model simulations, including climatological and atmospheric features and the atmospheric teleconnections forced by ENSO, and model dynamics, which cause the internal biases, are described. Finally, model simulations are summarized and future further analyses are discussed in section 4.

2. Model and Data Set

2.1. Model Description

The GRIMs-CCM is a global and spherical harmonics version of GRIMs, which is coupled with the GEOS-Chem three-dimensional chemical transport model. GEOS-Chem is a global three-dimensional model of tropospheric chemistry (Bey et al., 2001), and the chemistry module of GRIMs-CCM is based on GEOS-Chem v9-01-02 (http://acmg.seas.harvard.edu/geos/). The GRIMs produces the meteorology that drives emission, deposition, chemistry, and transport of chemical tracers in the chemistry module. On one hand, the chemistry module produces mass concentrations of various aerosols including sulfate, ammonium, nitrate, organic aerosol, black carbon, sea salt, and dust. Based on their mass concentrations, the chemical module assumes their size distribution and calculates the aerosol optical depth, single-scattering albedo, and asymmetry parameter through MIE theory. Subsequently, this information is used in radiation transfer calculation in GRIMs. In other words, the calculated tropospheric ozone and aerosol concentrations are used in

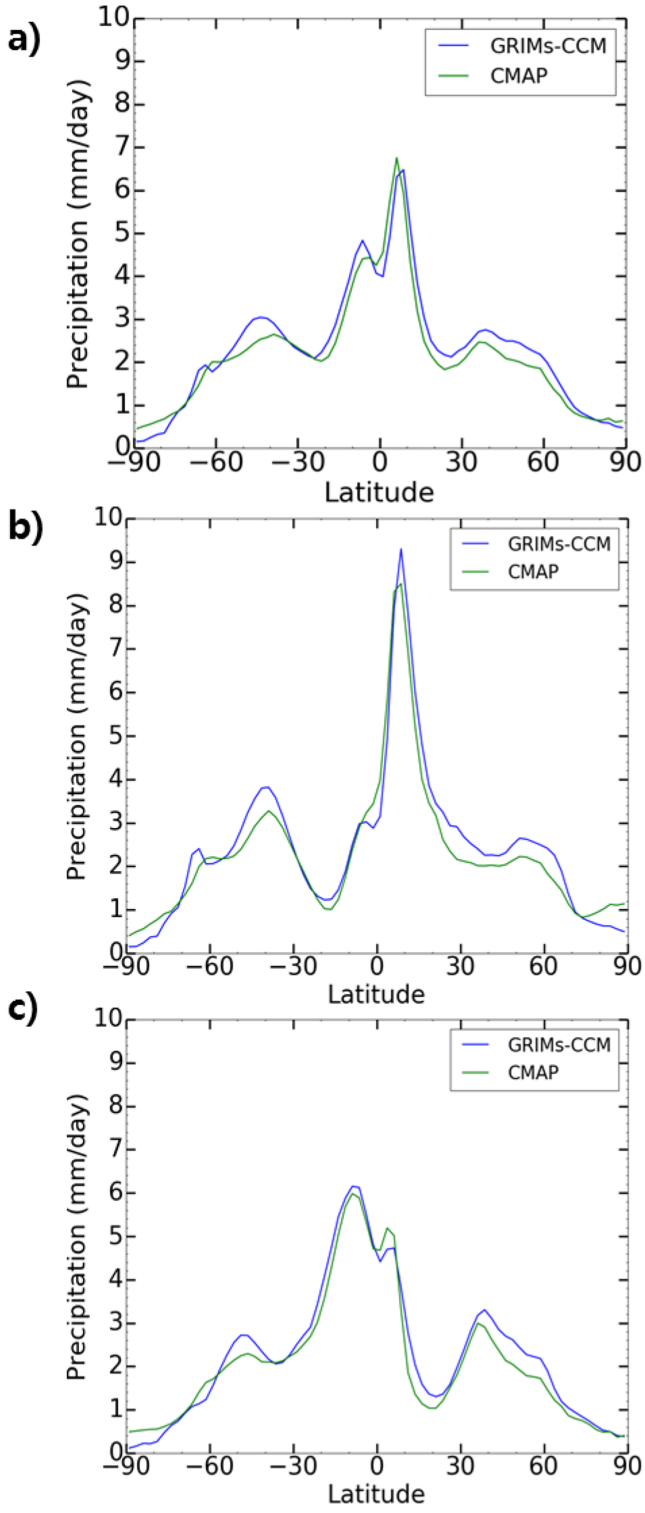

Figure 1. Zonally averaged annual, JJA, and DJF (Figures 1a–1c, respectively) precipitation rates (mm/day) for GRIMS-CCM and CMAP data. The blue line for GRIMs-CCM and the green line for CMAP.

the calculation of radiative flux as they make perturbations in the radiation balance by absorbing or scattering incoming solar radiation. Through this coupling of GRIMs and the chemistry module, GRIMs-CCM can simulate the atmospheric responses arising from the radiative direct effects of aerosols. It should be noted that GRIMs-CCM is designed to simulate aerosol direct effect only. The physics package of the GRIMs-CCM used in this study is based on version 3.2, which employs the advanced physics components of the Weather Research Forecast model. The reader is referred to Hong et al. (2013) for more details about physics version 3.1, and we slightly modified the physics package including schemes for convection, radiation, and gravity wave drag (Table 1).

2.2. GRIMs-CCM Experiment

Integration of the GRIMs-CCM was undertaken using the CCMI standard set of specific forcings (Eyring et al., 2013) with resolution T62 and L47 and with 20-min time steps to evaluate GRIMs-CCM's general performance. We used SST and SIC from the Hadley Centre Sea Ice and Sea Surface Temperature (HadISST) monthly data set (Rayner, 2003) as boundary conditions to force GRIMs from 1950 to 2010. For GHG concentrations, the CMIP5 recommended data (Meinshausen et al., 2011) were applied until 2005 and the RCP 8.5 scenario (Riahi et al., 2011) was applied after 2005. Among all possible GHGs, CO_2, CH_4, N_2O, CFC-11, CFC-12, CFC-22, and CCl_4 were considered in the radiation model. For anthropogenic and biomass burning, the Monitoring of Atmospheric Composition and Climate (MACC; Hollingsworth et al., 2008) and CityZen (MACCity) emission data sets (Granier et al., 2011) were used. Because biomass burning emissions are not available after 2008, the biomass burning emission data for 2008 were applied to the remainder of the period, that is, 2009 and 2010. Daily spectral solar irradiance data were taken from the Naval Research Laboratory Spectral Solar Irradiance model (Lean et al., 2005), and they were spectrally integrated to total solar irradiance and used in the Rapid Radiative Transfer Model for GCMs model.

Because GRIMs-CCM does not include interactive stratospheric chemistry, the stratospheric aerosol and ozone concentrations were prescribed. We prescribed monthly zonal mean surface area densities for stratospheric aerosols and the AC&C/Stratosphere-troposphere Processes And their Role in Climate ozone database (Cionni et al., 2011) for stratospheric ozone (Eyring et al., 2013). Among the CCMI REF-C1 standard forcing recommendations, Ozone Depleting Substances and Very Short-Lived Species were not used in the simulation because GRIMs-CCM does not include representation of the chemical reactions for those. The Ozone Depleting Substances, which are also GHGs such as CFC-11, CFC-12, CFC-22, and CCl_4, were only considered in the calculation of radiation. The additional CCMI forcing data descriptions are well described in Morgenstern et al. (2017).

To examine the effects of coupled chemical processes in climate system, we conducted additional experiment using GRIMs without CCM (hereafter referred to as GRIMs-CCM-off). While all forcings and boundary conditions were identical to CCMI REF-C1 experiment, monthly climatological aerosols concentrations and tropospheric ozone obtained from GRIMs-CCM were prescribed in GRIMs-CCM-off. Therefore, the difference between GRIMs-CCM and GRIMs-CCM-off is limited to the effects of chemistry-climate coupled processes.

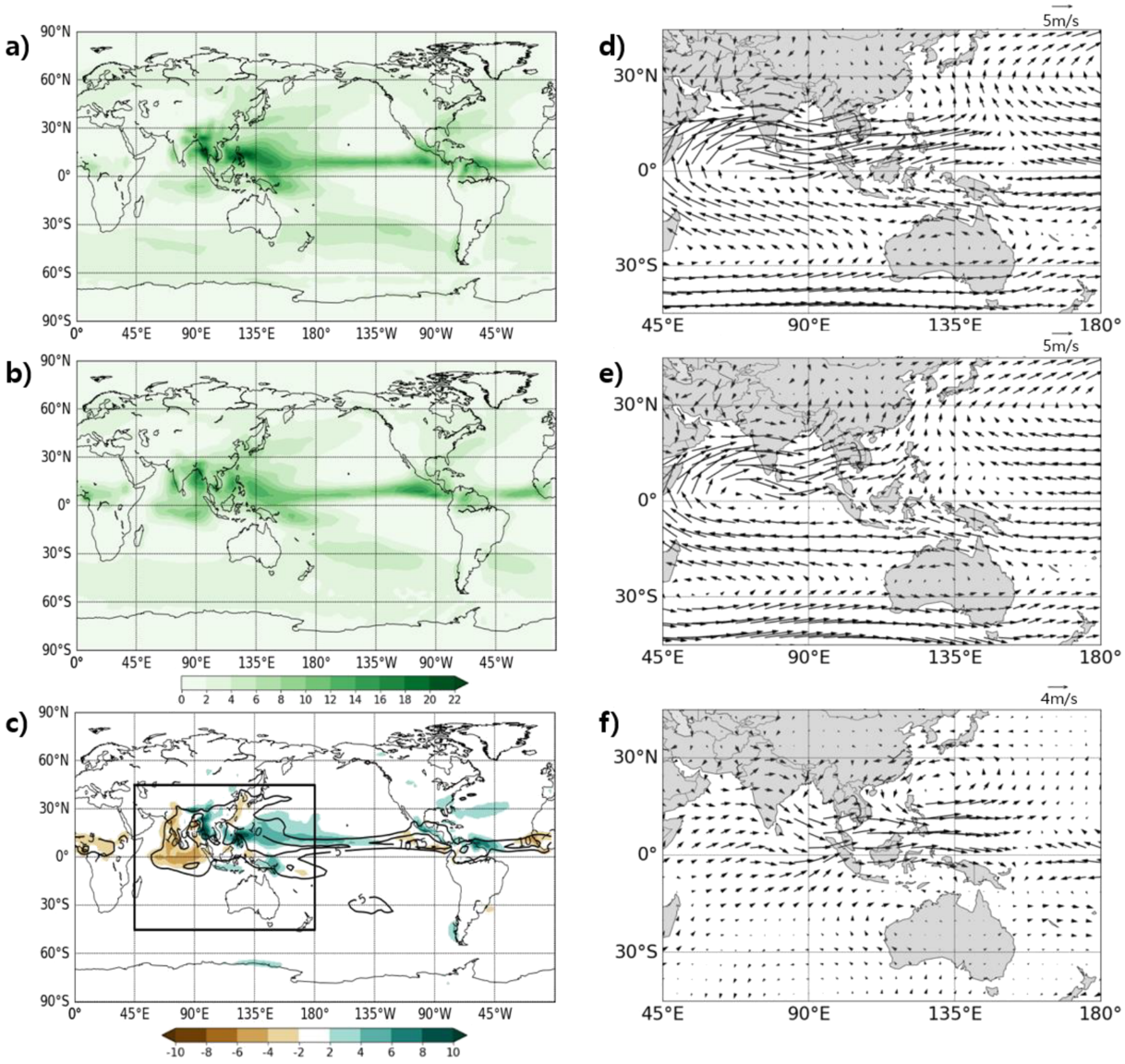

Figure 2. Shaded areas for global distributions of precipitation (mm/day) during JJA (1979–2010) for (a) GRIMs-CCM, (b) CMAP, and (c) precipitation bias (GRIMs-CCM minus CMAP). The contours in Figure 2c indicate the CMAP climatology (mm/day) on the same period. The black box region (45°E–180°E, 45°S–45°N) in Figure 2c is the region where GRIMs-CCM has noticeable biases. The 850-hPa winds over the black box region during JJA for GRIMs-CCM, NCEP/NCAR reanalysis, and 850-hPa wind bias in GRIMs-CCM are presented in Figures 2d–2f, respectively.

2.3. Reference Data Sets

The results of integrations of the GRIMs-CCM were primarily compared to the National Center for Environmental Prediction/National Center for Atmospheric Research (NCEP/NCAR) reanalysis 1 data (Kalnay et al., 1996) for 1960–2010 to examine its performance. Other data set used to examine GRIMs-CCM's performance includes the Climate Prediction Center merged analysis of precipitation (CMAP; Xie & Arkin, 1996) for 1979–2010. Furthermore, the SST data for ENSO composite analysis were obtained from the HadISST SST data set (Rayner, 2003), which was used as the boundary condition in REF-C1 simulations.

3. Results

3.1. Precipitation Simulations

First of all, zonal means of annual precipitation (1960–2010) during boreal summer (June-July-August, hereafter, JJA) and boreal winter (December-January-February, hereafter, DJF) of the GRIMs-CCM and

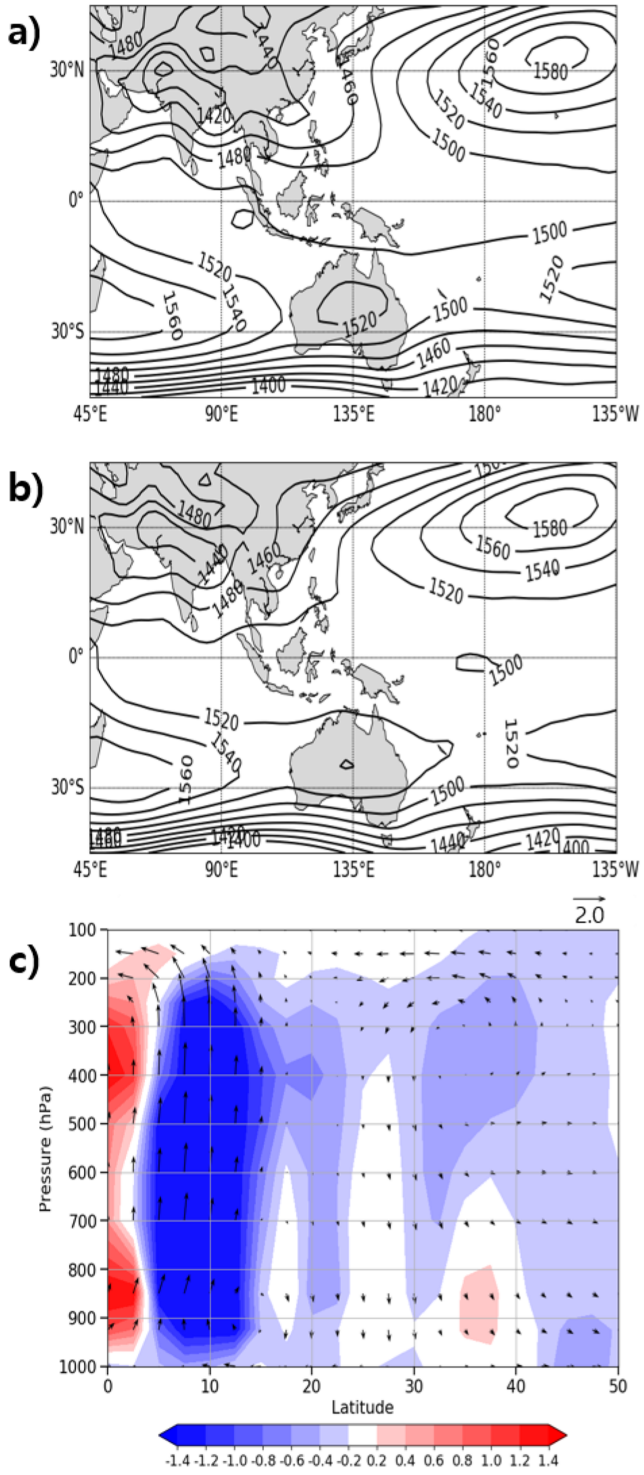

Figure 3. The 850-hPa geopotential height (GPH850) during JJA for (a) GRIMs-CCM and (b) NCEP/NCAR reanalysis. The contour intervals in Figures 3a and 3b are 20 m. (c) The NCEP/NCAR zonal mean vertical winds (*vector*) and the difference (GRIMs-CCM minus NCEP/NCAR reanalysis) of the vertical velocity (Pa/s, shading). Each wind component is zonally averaged (135°E to 120°W), and the vertical velocity components are 100 times greater than its original values. The negative (*positive*) in Figure 3c indicates stronger (*weaker*) upward motions in GRIMs-CCM than in NCEP/NCAR reanalysis.

CMAP were calculated, respectively (Figure 1). While the main features of zonal mean annual precipitation rates were captured by GRIMs-CCM compared with observations, GRIMs-CCM tended to simulate larger precipitation rates in the midlatitudes in both hemispheres (Figure 1a). It was found that the location of peak maximum annual mean precipitation was slightly shifted to the north in GRIMs-CCM compared to that in CMAP (Figure 1a), indicating that the latitudinal position of the ITCZ in the Northern Hemisphere (NH) was slightly shifted to the north in GRIMs-CCM compared with observations. The migration of seasonal precipitation in both hemispheres from summer to winter in both was captured in the GRIMs-CCM compared to the observations.

Figures 2a and 2b show the global distributions of precipitation during JJA in GRIMs-CCM and CMAP data sets, respectively, and Figure 2c displays their difference (GRIMs-CCM minus CMAP). During JJA, there were significant differences near the Philippines and over the Indochina peninsular in GRIMs-CCM compared to observations (Figures 2a–2c). In both regions, GRIMs-CCM overestimated precipitation amount compared to CMAP data. This contrasts with the Indian Ocean where the GRIMs-CCM underestimated the amount of precipitation.

To understand the difference between GRIMs-CCM and CMAP data sets during JJA, we examined the low-level (850 hPa) winds in GRIMs-CCM and NCEP/NCAR reanalysis (Figures 2d–2f). Precipitation over Philippines and the Indochina peninsular is largely affected by the ITCZ and the Indian monsoon or the Western North Pacific (WNP) monsoon in JJA. The GRIMs-CCM simulated stronger westerly winds prevailing over the Philippine Sea compared to the NCEP/NCAR reanalysis (Figure 2f), which were mainly associated with stronger summer monsoon flows over the north Indian Ocean in GRIMs-CCM compared with the reanalysis. Furthermore, weaker southerly winds over the East and South China Sea in GRIMs-CCM made the cyclonic structure in the WNP (Figure 2f), which acted to increase the amount of precipitation in this region. That is, stronger westerly winds over the Indian Ocean enhanced local evaporation and transport of water vapor into the WNP, resulting in more precipitation (Chou et al., 2003). Strong westerly winds over in the WNP decelerated, which caused low-level convergence (Figure 2f; Murakami & Matsumoto, 1994). This also contributed to enhance the amount of precipitation in the WNP in GRIMs-CCM compared to the observations.

In addition, the trough-like pattern extended to the WNP in GRIMs-CCM but not in NCEP/NCAR reanalysis. In addition, the North Pacific High over the North Pacific in NCEP/NCAR reanalysis extended more to the Asian continent than in the GRIMs-CCM (Figures 3a and 3b). The weak North Pacific High is associated with strong westerly winds over the WNP region (Murakami & Matsumoto, 1994), which is consistent with a weak North Pacific High in the GRIMs-CCM. In fact, the GRIMs-CCM simulated stronger convection in the tropics but weaker downward motion in midlatitudes (about 30°N) between 135°E and 120°W where the North Pacific High exists (Figure 3c). Therefore, underestimating the downward motion over the midlatitude of the North Pacific region caused a weak North Pacific High and strong westerly winds over the WNP region and finally resulted in overestimating the amount of precipitation over the WNP region in the GRIMs-CCM compared to the NCEP/NCAR reanalysis.

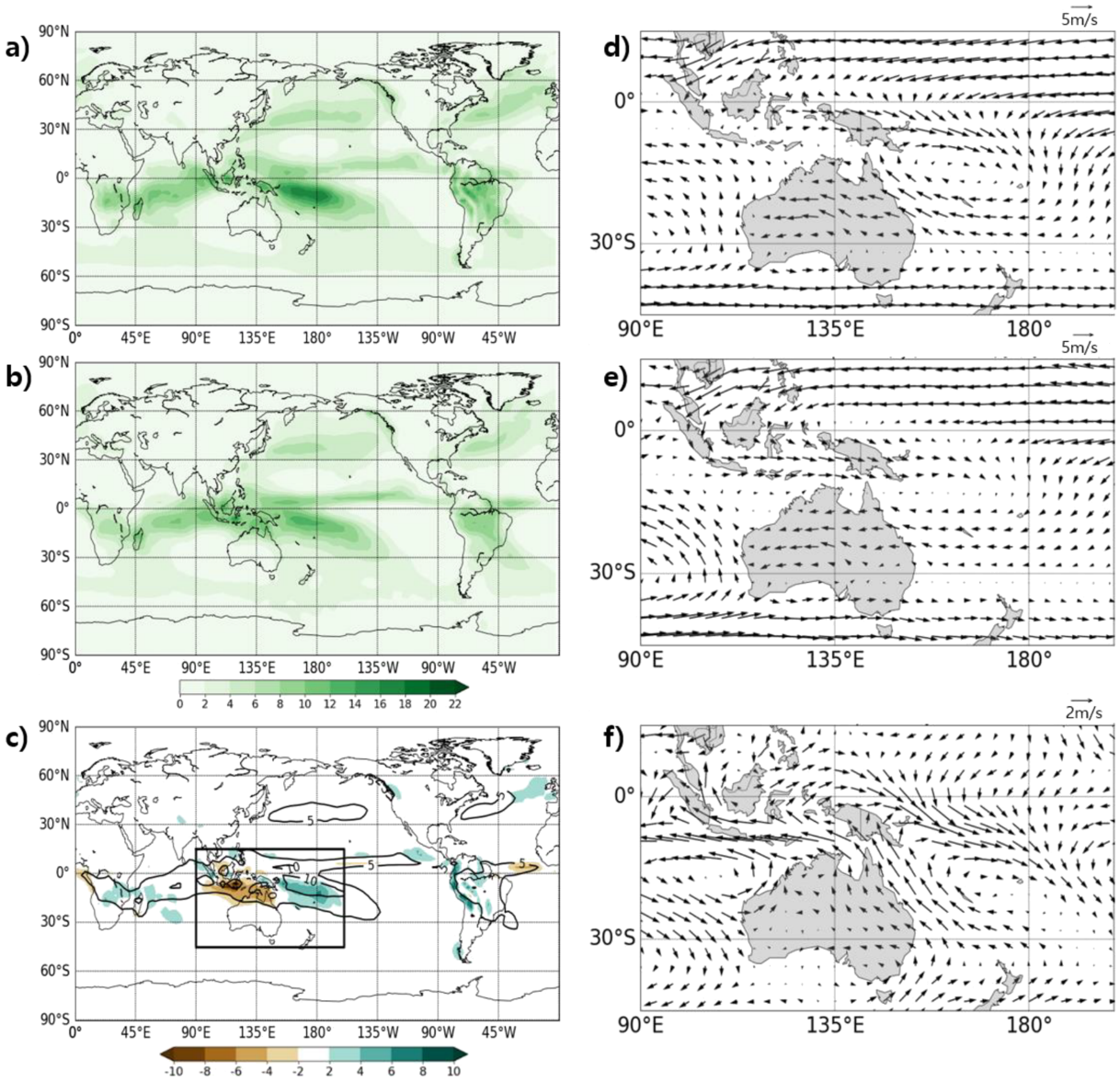

Figure 4. The same as in Figure 2 but during DJF. The black box region is 90°E–200°E, 45°S–15°N.

The global distributions of precipitation during DJF in GRIMs-CCM and CMAP data sets are shown in Figures 4a and 4b. Despite the fact that the GRIMs-CCM reasonably simulated the spatial pattern of precipitation over most regions, it overestimated precipitation over the South Pacific Convergence Zone (SPCZ) and underestimated precipitation over the Maritime Continents (Figure 4c). To understand the precipitation bias over the SPCZ, in particular, we analyzed the low-level (850 hPa) wind in the GRIMs-CCM and NCEP/NCAR reanalysis (Figures 4d–4f). We found that that the GRIMs-CCM simulated stronger low-level (850 hPa) wind over the SPCZ compared to the NCEP/NCAR reanalysis (Figures 4d–4f) and, consistently, tended to simulate much stronger low pressures over east New Guinea (Figure 5a). This was not observed in NCEP/NCAR reanalysis (Figure 5b), which is associated with less precipitation over the SPCZ compared to the GRIMs-CCM (Figure 4c). It is noteworthy that strong low pressure over the SPCZ is associated with much warmer surface temperature in Australia (Kodama, 1993). Similarly, GRIMs-CCM overestimated the surface temperature in Australia relative to the reanalysis (Figure 5c). Warmer land temperatures caused a warmer atmosphere via sensible heat flux (Figure 5d), which contributed to the formation of low pressure, especially over northern Australia.

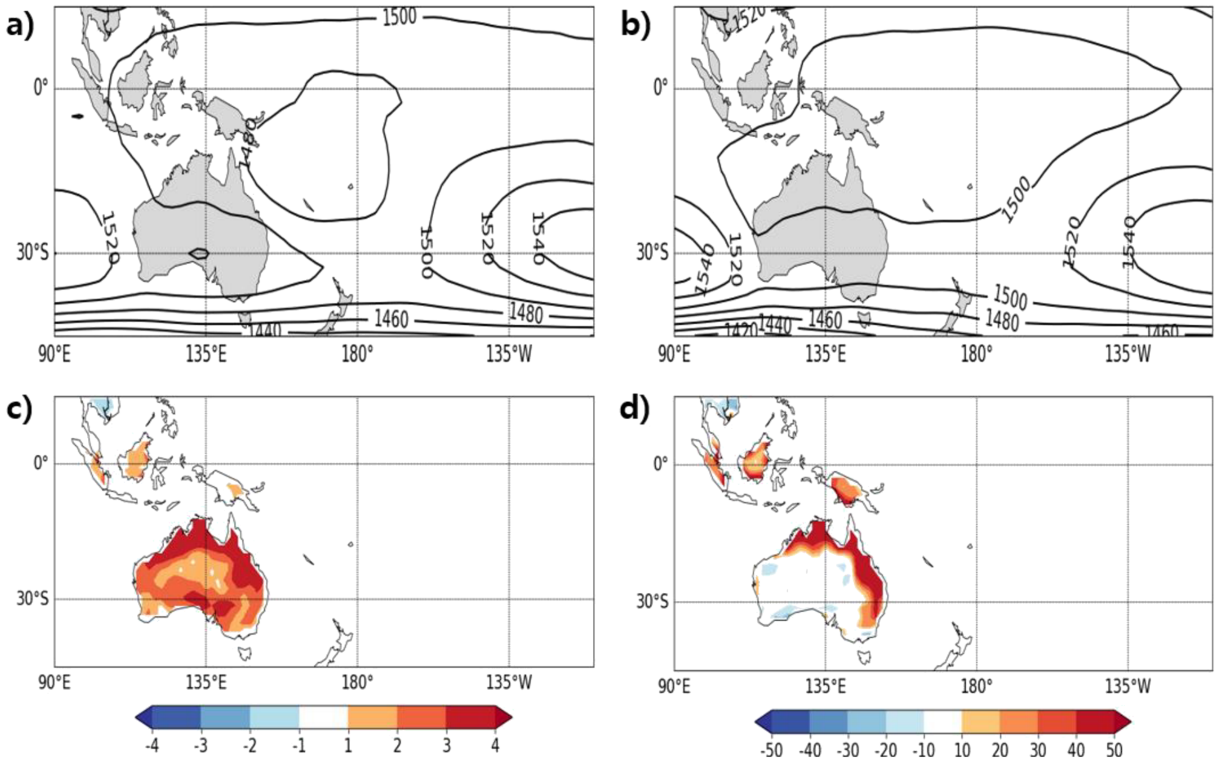

Figure 5. The GPH850 over the western South Pacific during DJF for (a) GRIMs-CCM and (b) NCEP/NCAR reanalysis. The contour intervals in Figures 5a and 5b are 20 m. The surface temperature bias (°C) (GRIMs-CCM minus NCEP/NCAR reanalysis) and the sensible heat flux bias (W/m^2) are presented in Figures 5c and 5d, respectively. Shading intervals are 1 °C in Figure 5c and 10 W/m^2 in Figure 5d.

3.2. Temperature Simulations

As mentioned in the above section, the GRIMs-CCM tended to simulate warmer land temperatures in Australia than the NCEP/NCAR reanalysis. We further examined the physical processes associated with the warmer surface temperature bias in Australia in the GRIMs-CCM compared to the reanalysis data set. The GRIMs-CCM simulated 44.0% total cloud cover in Australia during DJF, but 48.6% was simulated in NCEP/NCAR reanalysis. This resulted in a 5.8% increase in incident short-wave radiation over Australia in the GRIMs-CCM compared to NCEP/NCAR reanalysis during DJF (Table 2), thereby causing the warmer temperature bias in Australia during the Austral summer.

To further examine the characteristics of air temperature simulated in the GRIMs-CCM, we calculated the difference of zonally (0–360°E) averaged temperature in four seasons between the GRIMs-CCM and the NCEP/NCAR reanalysis (GRIMs-CCM minus NCEP/NCAR reanalysis; Figure 6). Although the GRIMs-CCM reasonably simulated the tropospheric air temperatures in midlatitudes and low latitudes, warm and cold biases in high latitudes in both hemispheres were apparent. In particular, a large cold bias in the upper and lower stratosphere occurred in every season. Furthermore, a warm bias in the lower troposphere was observed in both hemispheres, with the exception of the warm season in each hemisphere (i.e., JJA in Northern Hemisphere and DJF in Southern Hemisphere).

Table 2
The Area-Averaged (110°E–155°E and 45°S–10°S) Downward Short-Wave Radiation at Surface ($Fs_{\downarrow}$) and Total Cloud Cover (TCC) for the GRIMs-CCM, NCEP/NCAR Reanalysis, and Difference (GRIMs-CCM Minus NCEP/NCAR Reanalysis) During DJF

	GRIMs-CCM	NCEP/NCAR reanalysis	Difference	Difference (%)
$Fs_{\downarrow}$ (W/m^2)	310.1	293.0	17.1	5.82
TCC (%)	44.0	48.6	−4.6	−9.30

Note. The difference (%) is the difference value relative to NCEP/NCAR reanalysis.

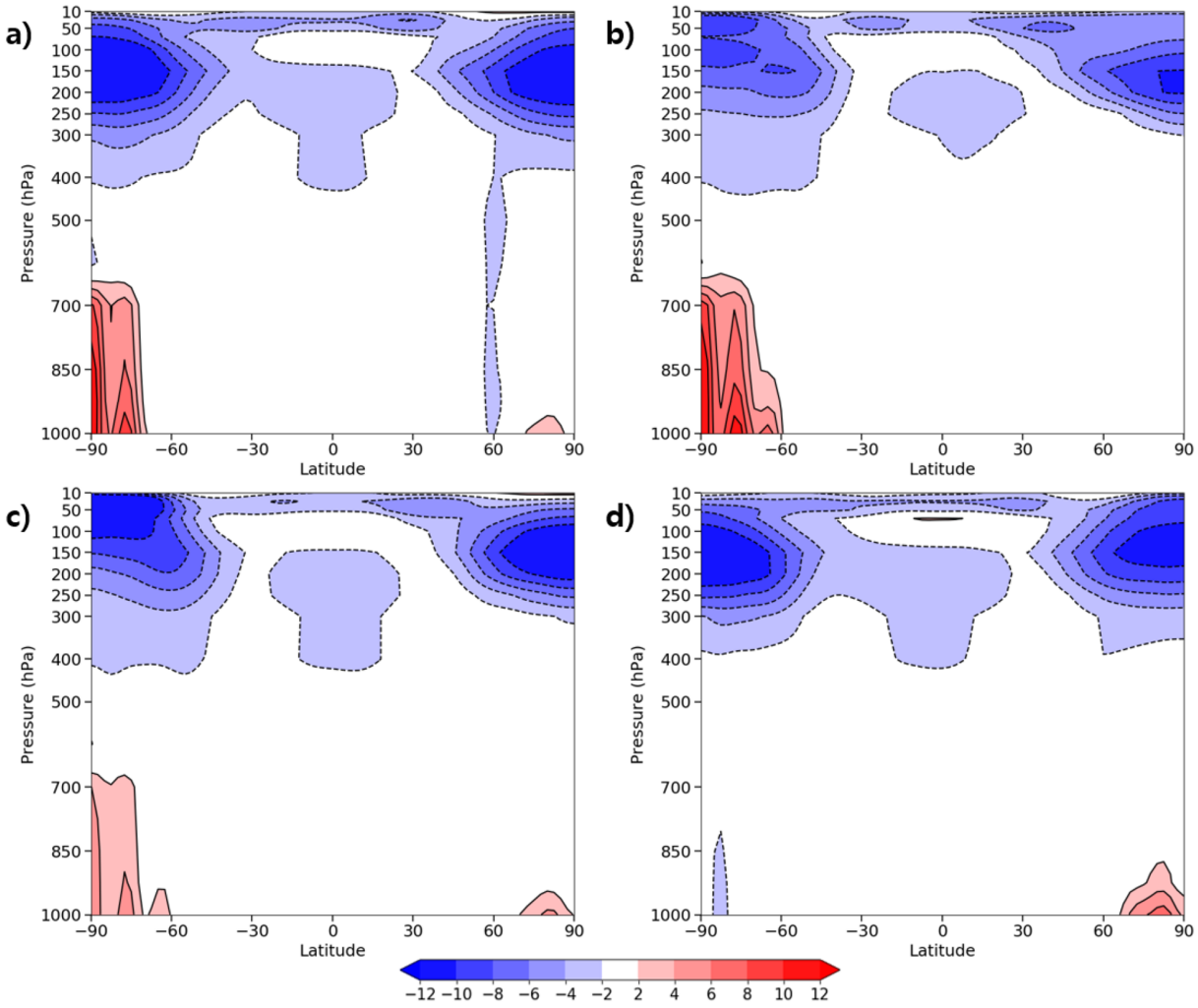

Figure 6. Seasonal zonally averaged vertical profiles of air temperature (°C) biases (GRIMs-CCM minus NCEP/NCAR reanalysis) for (a) MAM, (b) JJA, (c) SON, and (d) DJF. The contour intervals are 2 °C, and zero contours are omitted.

Most current chemistry-climate models tend to simulate the *cold pole problem* in the stratosphere, and such temperature biases arise because of an unsatisfactory wave propagation or a failure to represent the heat flux-temperature relationship, or both, in models (Austin et al., 2003; Newman et al., 2001). Representation of the wave's propagation can be affected by the horizontal resolution utilized in climate models. Although low-resolution models can resolve a low-amplitude wave along with small heat fluxes, they usually have a low capability of capturing a large heat flux, along with its possibly significant potential enstrophy cascade to larger wave numbers (Austin et al., 2003). Therefore, the GRIMs-CCM, having a coarse horizontal resolution, was unable to accurately simulate the heat flux-temperature relationship. Furthermore, chemistry-climate models that employ the nonorography gravity wave drag scheme tend to reduce such temperature biases, especially in the Southern Hemisphere stratosphere (Austin et al., 2003; Manzini et al., 1997). This is in contrast to the GRIMs-CCM, which incorporates an orographic flow-blocking gravity wave drag scheme.

In this study, we mainly focused on understanding which processes cause the temperature biases in GRIMs-CCM in the lowest level of the atmosphere (i.e., 1,000 hPa), in particular, biases over the Antarctic during JJA (Figure 6b). During JJA, the GRIMs-CCM simulated more net radiation (shadings) equal to about 10–50 W/m^2 (Figure 7a). More incident radiation resulted in warm biases over the Antarctic. These positive net radiation differences resulted from a positive downward long-wave radiation difference (Figure 7b); the pattern of net radiation was very similar to that of downward long-wave radiation. We argue that the

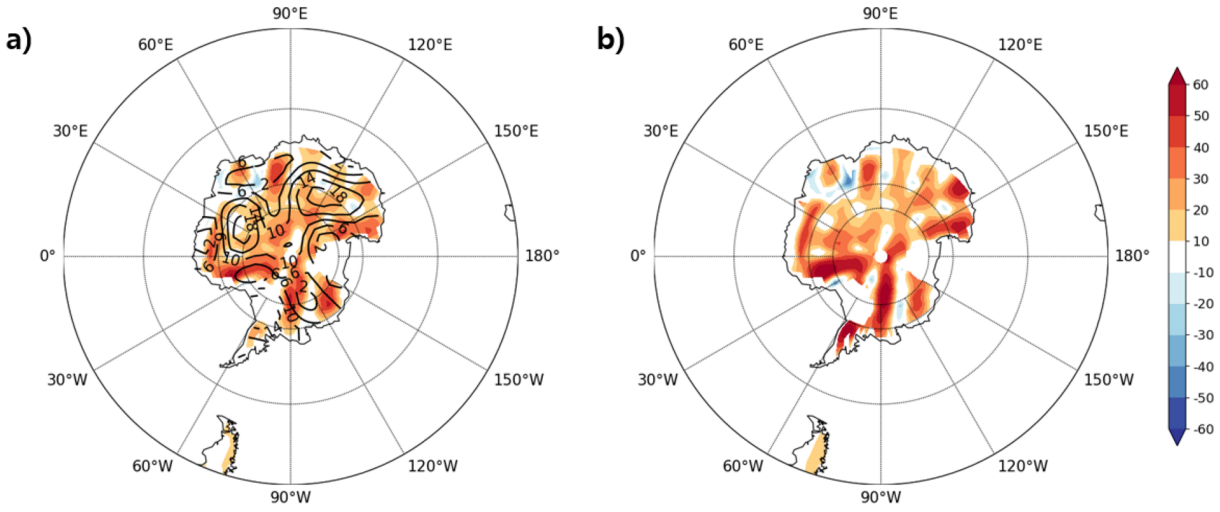

Figure 7. (a) Temperature bias (contours, °C) and net radiation bias (shadings, W/m^2) over the Antarctic during JJA and (b) downward long-wave radiation bias. Positive downward long-wave radiation bias means more downward long-wave in GRIMs-CCM. The contour interval in Figure 7a is 4 °C, and shading intervals in both Figures 7a and 7b are 10 W/m^2.

difference in water vapor pressure in the atmosphere may cause the difference in net radiation balance by modulating the long-wave radiation balance in the GRIMs-CCM compared to the reanalysis dataset. Water vapor pressure in the atmosphere was represented in many ways in the model, including total column precipitable water (TPW), relative humidity, and specific humidity. TPW is a parameter that represents the absolute water vapor content in an entire atmosphere column. The area averaged (0–360°E and 90–60°S) TPW of GRIMs-CCM was 20.8% larger than that of NCEP/NCAR reanalysis, indicating that more water vapor in the atmosphere would cause a stronger greenhouse effect in the GRIMs-CCM compared to that of the NCEP/NCAR reanalysis (Table 3). This resulted in more downward long-wave radiation and a warmer Antarctic during JJA in the GRIMs-CCM.

3.3. Atmospheric Teleconnections in Response to ENSO

ENSO is a prominent climate fluctuation and affects many regions outside the tropical Pacific through its atmospheric teleconnections (Bjerknes, 1969; Diaz et al., 2001; McPhaden et al., 2006; Stan et al., 2017; Trenberth et al., 1998; Yeh et al., 2018). Therefore, it is useful to examine the atmospheric circulation in response to ENSO to estimate the performance of the GRIMs-CCM. El Niño years are defined as years when the Nino3.4 index exceeds 0.5 °C, and La Niña years are defined as years when the Nino3.4 index is below −0.5 °C (Table 4). Note that Nino3.4 index is defined as the detrended SST anomaly averaged in the Nino3.4 region (190°W–120°W, 5°N–5°S) during DJF from 1960 to 2010. We conducted a composite analysis to examine atmospheric teleconnections during El Niño and La Niña years in GRIMs-CCM during DJF, and then we compared the results with the reanalysis data.

A typical atmospheric teleconnection due to ENSO is known as the Pacific/North American (PNA) and Pacific/South American (PSA) patterns (Horel & Wallace, 1981; Karoly, 1989; Yeh et al., 2018). In El Niño years, for example, a positive GPH anomaly exists over the tropical Pacific and North America and a negative anomaly occurs over the North Pacific and Southeast North America, and vice versa in La Niña years. Similarly, the PSA patterns in both El Niño and La Niña years have symmetric structures in anomalies to the PNA patterns but the magnitude of the anomaly is smaller than that in the Northern Hemisphere.

Table 3
The Area Averaged (0°–360°E and 90°S–60°S) Total Column Precipitable Water (TPW) for GRIMs-CCM, NCEP/NCAR Reanalysis, and Difference (GRIMs-CCM Minus NCEP/NCAR Reanalysis)

kg/m^2	GRIMs-CCM	NCEP/NCAR reanalysis	Difference	Difference (%)
TPW	3.14	2.60	0.54	20.77

Note. The difference (%) is the difference value relative to NCEP/NCAR reanalysis.

The PNA patterns simulated in the GRIMs-CCM during El Niño and La Niña years were comparable with those in the reanalysis during DJF (Figure 8). The pattern correlations between GRIMs-CCM and NCEP/NCAR reanalysis were 0.84 in El Niño years and 0.70 in La Niña years, respectively. However, there were slight differences in the

Table 4
The El Niño and the La Niña Years From Nino3.4 Indices

	Years
El Niño	1963, 1965, 1968, 1969, 1972, 1976, 1977, 1979, 1982, 1986, 1987, 1991, 1994, 1997, 2002, 2004, 2006, and 2009
La Niña	1964, 1967, 1970, 1971, 1973, 1974, 1975, 1983, 1984, 1985, 1988, 1995, 1998, 1999, 2000, 2005, 2007, and 2008

magnitude of GPH500 anomalies in both hemispheres. In El Niño years, for example, the intensity of the Aleutian low-pressure system in the North Pacific was stronger in the GRIMS-CCM than in the reanalysis. In addition, the center of the Aleutian low-pressure system was slightly shifted to the west in the GRIMs-CCM compared to the reanalysis. In contrast, a PSA-like atmospheric teleconnection was more prominent in the Southern Hemisphere in the GRIMs-CCM compared to the reanalysis (Figures 8a and 8b). It is also noteworthy that the intensity of PSA-like atmospheric teleconnections was stronger in the GRIMs-CCM than the reanalysis. The spatial structures of GPH500 during La Niña (Figures 8c and 8d) had both similarities and differences between the GRIMs-CCM and reanalysis. Stronger anomalous northwesterly winds and southwesterly winds were simulated over America in GRIMS-CCM, than with the reanalysis. The existence of anomalous high pressure over the Atlantic in the GRIMs-CCM was also noticeable. In spite of these, a propagation of Rossby waves and the overall PNA patterns were well simulated in the GRIMs-CCM and comparable with the reanalysis.

Figure 9 is the same as Figure 8 except that composites of land temperatures at 1,000 hPa during DJF were used in Figure 9. The overall pattern of land temperature was reasonably simulated in the GRIMs-CCM compared to the reanalysis data set. In El Niño years (Figures 9a and 9b), the GRIMs-CCM captured the anomalous warm in Alaska and northwest Canada and the anomalous cold in southeast North America. In those regions, the GRIMs-CCM tended to overestimate both positive and negative temperature anomalies. The

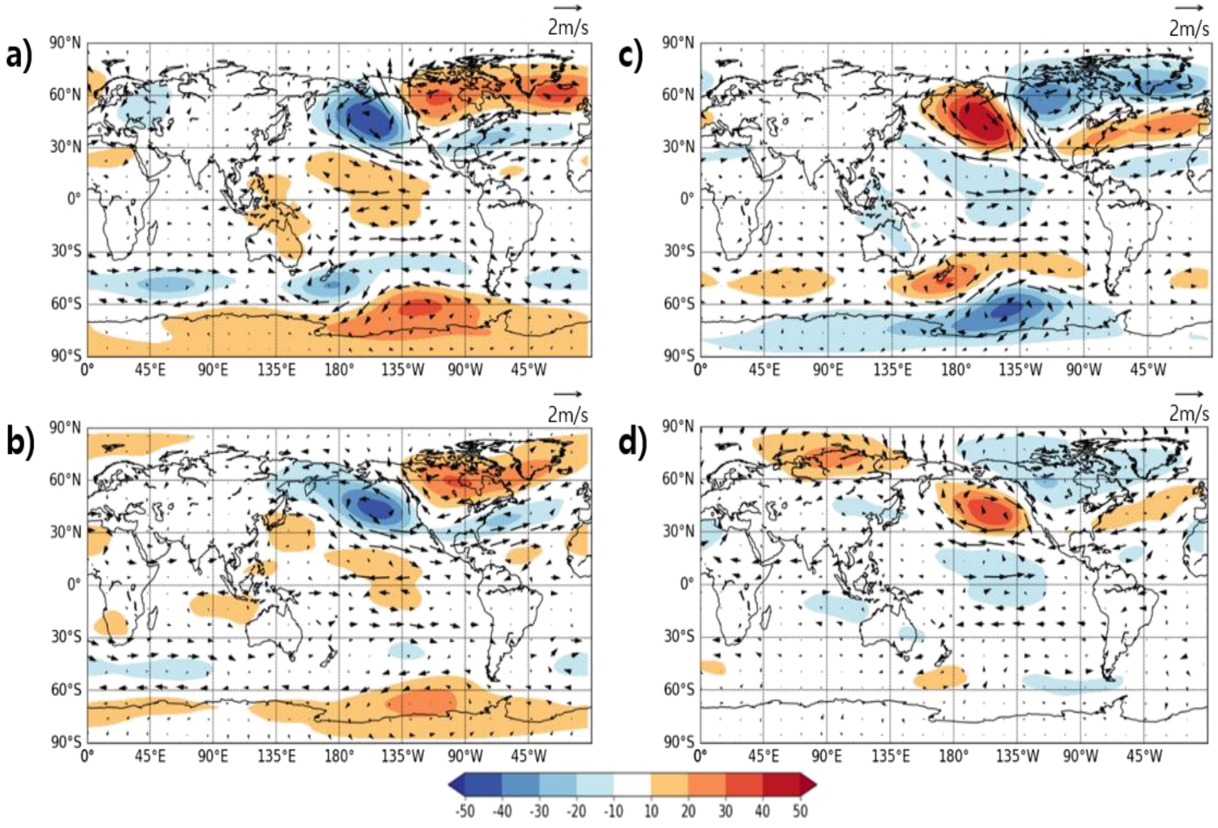

Figure 8. Shaded areas for composite of GPH500 anomaly (m) and vectors for composite of 500-hPa winds anomaly (m/s) during DJF for GRIMs-CCM (top) and NCEP/NCAR reanalysis (bottom). The left panel is for the El Niño years, and the right panel is for La Niña years.

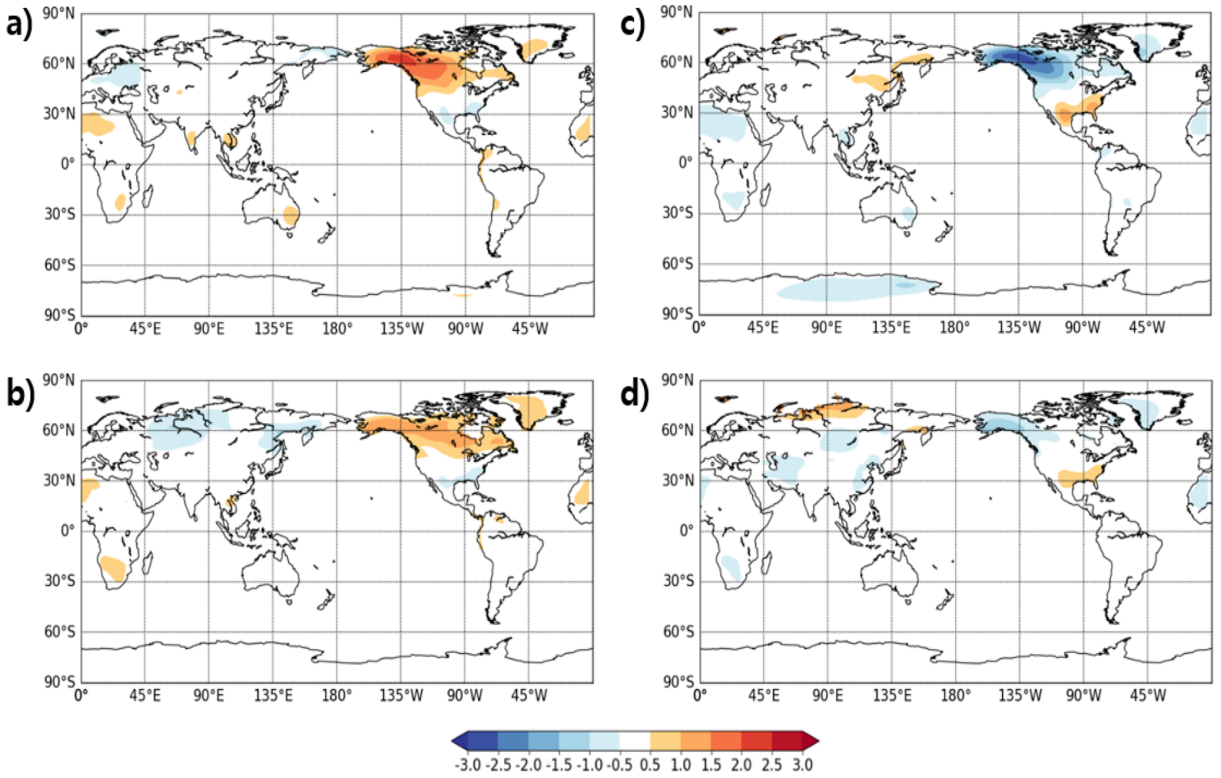

Figure 9. The same as Figure 8 but for the composite of 1,000-hPa air temperature (°C) over land.

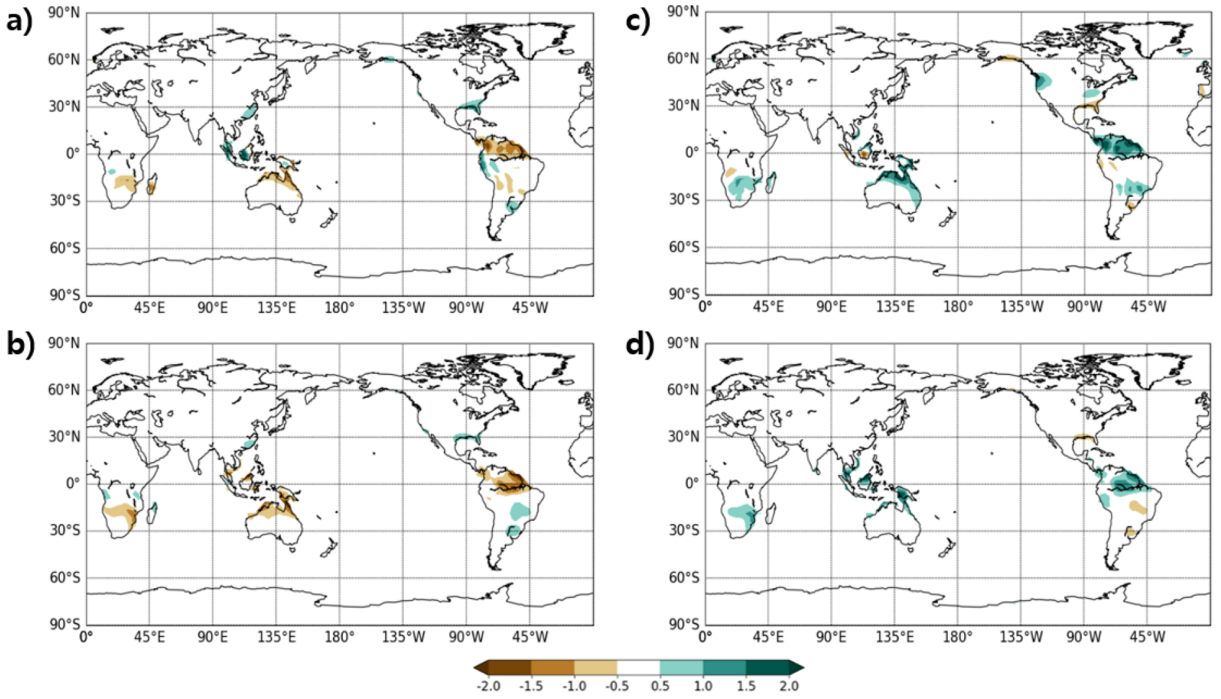

Figure 10. The same as in Figure 8 but for precipitation (mm/day) over land.

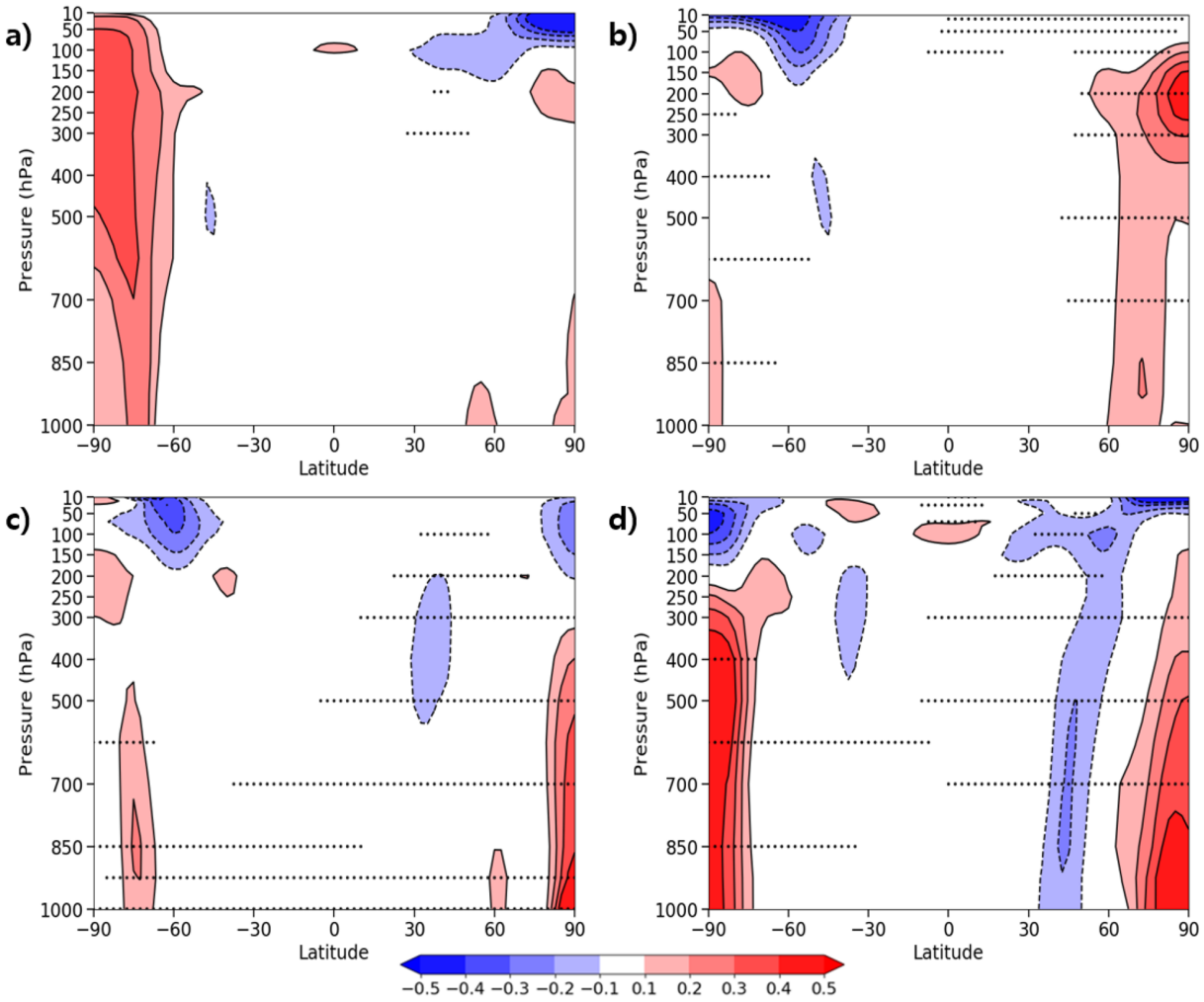

Figure 11. Seasonal zonally averaged vertical profiles of air temperature (°C) differences (GRIMs-CCM minus GRIMs-CCM-off) for (a) MAM, (b) JJA, (c) SON, and (d) DJF. The contour intervals are 0.1 °C, and zero contours are omitted. The black dot denotes the statistical significance at 95% confidence level based on the Student's *t* test.

overestimation of temperature anomalies was consistent with overestimation of GPH anomalies shown in Figure 8. In addition, there were some discrepancies of land temperature between the GRIMs-CCM and the reanalysis data set in Eurasia and Africa (Figures 9a and 9b). In contrast, in La Niña years (Figures 9c and 9d), the GRIMs-CCM captured the main features of land temperature in America but tended to overestimate both positive and negative anomalies. The composite analysis of temperature demonstrated that the GRIMs-CCM generally had a good estimation of temperature in response to ENSO in both North and South America, with slight difference in the remaining continents.

The GRIMs-CCM correctly simulated less precipitation in the northern part of South America and northern Australia in the El Niño years (Figures 10a and 10b). However, the GRIMs-CCM tended to overestimate the precipitation anomaly over the west coast of South America and Indonesia and underestimate the precipitation anomaly over central South America. In contrast, in the La Niña years (Figures 10c and 10d), precipitation anomalies were captured well by the GRIMs-CCM, although anomalous precipitation over the west coast of North America and central South America was overestimated.

3.4. Effects of Chemistry-Climate Coupled Processes in the GRIMs-CCM

To investigate the effects of chemistry-climate coupled processes in the GRIMs-CCM, we compared with two experiments (i.e., GRIMs-CCM with GRIMs-CCM-off). We found that the chemistry-climate coupled

processes were influential to the vertical structure of atmospheric temperature. In particular, such influences were dominant in high latitudes including poles in both hemispheres during JJA, SON, and DJF (Figure 11). The difference of tropospheric temperature due to chemistry-climate interaction was characterized by a warming in polar regions at both hemispheres during JJA, SON, and DJF (Figure 11). In particular, tropospheric temperature changes were the largest in both hemispheres during DJF (Figure 11d). On the other hand, the stratospheric cold pole problem (Austin et al., 2003) was not improved dramatically as compared with the temperature biases in GRIMs-CCM (see Figure 6). This indicates that the adopted physics scheme and horizontal resolution might be more important to improve the cold pole problem than the chemistry-climate coupled processes in the GRIMs-CCM. We also investigated the influence of chemistry-climate coupled processes on the precipitation simulated in GRIMs-CCM. Unlike the atmospheric temperature, the difference of precipitation between the two experiments was not statistically significant in most regions during four seasons (figure not shown), which might be associated with the fact that GRIMs-CCM is designed to simulate aerosol direct effect only.

4. Summary

We examined how well the GRIMs-CCM simulated a current (1960–2010) climate and analyzed how the coupled chemistry-climate processes influence the temperature and precipitation simulated in GRIMs-CCM under CCMI standard forcings. We found that the global distributions of various atmospheric features, including temperature, precipitation, and atmospheric circulation, were reasonably well simulated by the GRIMs-CCM although some noticeable regional systematic biases were apparent over specific regions.

While the seasonal migration of precipitation was reasonably simulated by the GRIMs-CCM, some regional biases, that is, more precipitation over the WNP during JJA and over the SPCZ during DJF, were observed. We argued that the underestimation of the North Pacific high during the boreal summer may lead to a more eastward incursion of westerly winds and cause more convection and rainfall in the GRIMs-CCM. In fact, it is known that the WNP region has a negative correlation between precipitation and SST (Chou et al., 2003; Wang et al., 2001). The lack of an air-sea interaction in atmosphere-ocean uncoupled models, such as the GRIMs-CCM, might be partially responsible for the precipitation bias over this region. Meanwhile, during the Austral summer, the GRIMs-CCM slightly overestimated land surface temperatures in Australia, which caused low pressure and subsequently led to a larger pressure gradient and more convergence over the SPCZ, which in turn caused an overestimation of precipitation over the SPCZ. The GRIMs-CCM had the cold pole problem in the stratosphere, similar to that observed in other chemistry-climate models. This problem can be improved by increasing horizontal resolution within the model, along with employment of a gravity wave drag scheme. In troposphere, the GRIMs-CCM had a significant bias in overestimating temperature over the Antarctic during JJA. We investigated the physical processes underlying this warm bias and found that the difference in long-wave radiation balance due to differences in TPW contributed to the warmer Antarctic in the GRIMs-CCM. The GRIMs-CCM also had good performances under specific SST forcings, including both El Niño and La Niña years. The PNA pattern, which is the typical anomaly pattern of the ENSO teleconnection, was captured in the GRIMs-CCM. This indicated that changes in atmospheric teleconnections due to changes in deep convections were reasonably simulated in the GRIMs-CCM. However, the intensity and location of the anomalies of temperature and precipitation in response to ENSO were slightly different compared to the reanalysis data set. In addition, we investigated how the chemistry-climate coupled processes influence the temperature and precipitation simulated in GRIMs-CCM. We found that a significant effect of chemistry-climate coupled processes was limited in GRIMs-CCM, in particular, the tropospheric temperature in polar regions during DJF. On the other hand, the effect of chemistry-climate interaction on the simulated precipitation was insignificant.

Through CCMI hindcast reference simulation (REF-C1; Eyring et al., 2013) by GRIMs-CCM, we demonstrated that this newly developed GRIMs-CCM had a good ability to reproduce past climate satisfactorily compared to reanalysis data under CCMI standard forcings. The comparison of the GRIMs-CCM to NCEP/NCAR reanalysis gave us information about the characteristics of the performance of the GRIMs-CCM in both its climatological features and specific climate states, along with regional biases. The performance of GRIMs-CCM described in this study gives us a reliability of using GRIMs-CCM not only in the present climate simulation but also in future climate simulation. Also, the information about some regional biases can help for other researchers to interpret the results in the GRIMs-CCM simulation. Further, by

adopting newly developed physics schemes such as a new convection scheme, it is necessary to enhance the performance of the GRIMs-CCM along with considering an indirect effect. This will be described in the part 2 for the current topic to introduce the GRIMs-CCM.

Acknowledgments
This study was supported by National Research Foundation Grant NRF-2018R1A5A1024958. Lee, S. and Park, R. J. were supported by the National Research Foundation of Korea (NRF) grant funded by the Korean government (MSIT) (No. 2018004494). The monthly NCEP/NCAR reanalysis 1 data and the CMAP data used in this study are available at National Oceanic and Atmospheric Administration (NOAA) Earth System Research Laboratory website (https://www.esrl.noaa.gov/psd/data/gridded/tables/monthly.html), and the monthly SST and SIC data set from HadISST can be downloaded at Met Office Hadley Centre website (https://www.metoffice.gov.uk/hadobs/hadisst/data/download.html). The available links of set of CCMI REF-C1 forcing data described in section are stated in Eyring et al. (2013). Also, the result of long-term integration using GRIMs-CCM under CCMI REF-C1 forcing can be downloaded at http://data.ceda.ac.uk/badc/wcrp-ccmi/data/CCMI-1/output/SNU-ACMG/GRIMs-CCM.

References

Austin, J., Shindell, D., Beagley, S., Brühl, C., Dameris, M., Manzini, E., et al. (2003). Uncertainties and assessments of chemistry-climate models of the stratosphere. *Atmospheric Chemistry and Physics*, *3*(1), 1–27. https://doi.org/10.5194/acp-3-1-2003

Bey, I., Jacob, D. J., Yantosca, R. M., Logan, J. A., Field, B. D., Fiore, A. M., et al. (2001). Global modeling of tropospheric chemistry with assimilated meteorology: Model description and evaluation. *Journal of Geophysical Research*, *106*(D19), 23,073–23,095. https://doi.org/10.1029/2001JD000807

Bjerknes, J. (1969). Atmospheric teleconnections from the equatorial Pacific. *Monthly Weather Review*, *97*(3), 163–172. https://doi.org/10.1175/1520-0493(1969)097<0163:ATFTEP>2.3.CO;2

Chang, E. C., Yeh, S. W., Hong, S. Y., & Wu, R. (2013). Sensitivity of summer precipitation to tropical sea surface temperatures over East Asia in the GRIMs GMP. *Geophysical Research Letters*, *40*, 1824–1831. https://doi.org/10.1002/grl.50389

Charlson, R. J., Schwartz, S., Hales, J., Cess, R. D., Coakley, J. J., Hansen, J., & Hofmann, D. (1992). Climate forcing by anthropogenic aerosols. *Science*, *255*(5043), 423–430. https://doi.org/10.1126/science.255.5043.423

Chen, F., & Dudhia, J. (2001). Coupling an advanced land surface–hydrology model with the Penn State–NCAR MM5 modeling system. Part I: Model implementation and sensitivity. *Monthly Weather Review*, *129*(4), 569–585. https://doi.org/10.1175/1520-0493(2001)129<0569:CAALSH>2.0.CO;2

Chou, C., Tu, J.-Y., & Yu, J.-Y. (2003). Interannual variability of the western North Pacific summer monsoon: Differences between ENSO and non-ENSO years. *Journal of Climate*, *16*(13), 2275–2287. https://doi.org/10.1175/2761.1

Cionni, I., Eyring, V., Lamarque, J.-F., Randel, W., Stevenson, D., Wu, F., et al. (2011). Ozone database in support of CMIP5 simulations: Results and corresponding radiative forcing. *Atmospheric Chemistry and Physics*, *11*(21), 11,267–11,292. https://doi.org/10.5194/acp-11-11267-2011

Diaz, H. F., Hoerling, M. P., & Eischeid, J. K. (2001). ENSO variability, teleconnections and climate change. *International Journal of Climatology*, *21*(15), 1845–1862. https://doi.org/10.1002/joc.631

Ek, M. B., Mitchell, K. E., Lin, Y., Rogers, E., Grunmann, P., Koren, V., et al. (2003). Implementation of Noah land surface model advances in the National Centers for Environmental Prediction operational mesoscale Eta model. *Journal of Geophysical Research*, *108*(D22), 8851. https://doi.org/10.1029/2002JD003296

Eyring, V., Lamarque, J.-F., Hess, P., Arfeuille, F., Bowman, K., Chipperfiel, M. P., et al. (2013). Overview of IGAC/SPARC Chemistry-Climate Model Initiative (CCMI) community simulations in support of upcoming ozone and climate assessments. *SPARC newsletter*, *40* (Januar), 48–66. http://oceanrep.geomar.de/id/eprint/20227

Granier, C., Bessagnet, B., Bond, T., D'Angiola, A., van Der Gon, H. D., Frost, G. J., et al. (2011). Evolution of anthropogenic and biomass burning emissions of air pollutants at global and regional scales during the 1980–2010 period. *Climatic Change*, *109*(1-2), 163–190. https://doi.org/10.1007/s10584-011-0154-1

Ham, S., Hong, S.-Y., & Park, S. (2014). A study on air–sea interaction on the simulated seasonal climate in an ocean–atmosphere coupled model. *Climate Dynamics*, *42*(5-6), 1175–1187.

Han, J., & Pan, H.-L. (2011). Revision of convection and vertical diffusion schemes in the NCEP global forecast system. *Weather and Forecasting*, *26*(4), 520–533. https://doi.org/10.1175/WAF-D-10-05038.1

Haywood, J., & Boucher, O. (2000). Estimates of the direct and indirect radiative forcing due to tropospheric aerosols: A review. *Reviews of Geophysics*, *38*(4), 513–543. https://doi.org/10.1029/1999RG000078

Hollingsworth, A., Engelen, R. J., Textor, C., Benedetti, A., Boucher, O., Chevallier, F., et al., & The Gems Consortium (2008). Toward a monitoring and forecasting system for atmospheric composition: The GEMS project. *Bulletin of the American Meteorological Society*, *89* (8), 1147–1164. https://doi.org/10.1175/2008BAMS2355.1

Hong, S.-Y., Dudhia, J., & Chen, S.-H. (2004). A revised approach to ice microphysical processes for the bulk parameterization of clouds and precipitation. *Monthly Weather Review*, *132*(1), 103–120. https://doi.org/10.1175/1520-0493(2004)132<0103:ARATIM>2.0.CO;2

Hong, S.-Y., Noh, Y., & Dudhia, J. (2006). A new vertical diffusion package with an explicit treatment of entrainment processes. *Monthly Weather Review*, *134*(9), 2318–2341. https://doi.org/10.1175/MWR3199.1

Hong, S.-Y., Park, H., Cheong, H.-B., Kim, J.-E. E., Koo, M.-S., Jang, J., et al. (2013). The Global/Regional Integrated Model system (GRIMs). *Asia-Pacific Journal of Atmospheric Sciences*, *49*(2), 219–243. https://doi.org/10.1007/s13143-013-0023-0

Horel, J. D., & Wallace, J. M. (1981). Planetary-scale atmospheric phenomena associated with the Southern Oscillation. *Monthly Weather Review*, *109*(4), 813–829. https://doi.org/10.1175/1520-0493(1981)109<0813:PSAPAW>2.0.CO;2

Iacono, M. J., Delamere, J. S., Mlawer, E. J., Shephard, M. W., Clough, S. A., & Collins, W. D. (2008). Radiative forcing by long-lived greenhouse gases: Calculations with the AER radiative transfer models. *Journal of Geophysical Research*, *113*, D13103. https://doi.org/10.1029/2008JD009944

Jang, J., & Hong, S.-Y. (2014). Quantitative forecast experiment of a heavy rainfall event over Korea in a global model: Horizontal resolution versus lead time issues. *Meteorology and Atmospheric Physics*, *124*(3-4), 113–127.

Jeong, J. I., & Park, R. J. (2017). Winter monsoon variability and its impact on aerosol concentrations in East Asia. *Environmental Pollution*, *221*, 285–292. https://doi.org/10.1016/j.envpol.2016.11.075

Jeong, J. I., Park, R. J., & Yeh, S.-W. (2018). Dissimilar effects of two El Niño types on $PM_{2.5}$ concentrations in East Asia. *Environmental pollution*, *242*, 1395–1403.

Kalnay, E., Kanamitsu, M., Kistler, R., Collins, W., Deaven, D., Gandin, L., et al. (1996). The NCEP/NCAR 40-year reanalysis project. *Bulletin of the American meteorological Society*, *77*(3), 437–471. https://doi.org/10.1175/1520-0477(1996)077<0437:TNYRP>2.0.CO;2

Karoly, D. J. (1989). Southern Hemisphere circulation features associated with El Niño-Southern Oscillation events. *Journal of Climate*, *2*(11), 1239–1252. https://doi.org/10.1175/1520-0442(1989)002<1239:SHCFAW>2.0.CO;2

Kiehl, J., & Briegleb, B. (1993). The relative roles of sulfate aerosols and greenhouse gases in climate forcing. *Science*, *260*(5106), 311–314. https://doi.org/10.1126/science.260.5106.311

Kim, J.-W., Yeh, S.-W., & Chang, E.-C. (2014). Combined effect of El Niño-Southern Oscillation and Pacific decadal oscillation on the East Asian winter monsoon. *Climate Dynamics*, *42*(3-4), 957–971.

Kim, M. J., Yeh, S. W., & Park, R. J. (2016). Effects of sulfate aerosol forcing on East Asian summer monsoon for 1985–2010. *Geophysical Research Letters*, *43*, 1364–1372. https://doi.org/10.1002/2015GL067124

Kim, Y. j., & Doyle, J. D. (2005). Extension of an orographic-drag parametrization scheme to incorporate orographic anisotropy and flow blocking. *Quarterly Journal of the Royal Meteorological Society: A Journal of the Atmospheric Sciences, Applied Meteorology and Physical Oceanography*, *131*(609), 1893–1921. https://doi.org/10.1256/qj.04.160

Kodama, Y.-M. (1993). Large-scale common features of sub-tropical convergence zones (the Baiu Frontal Zone, the SPCZ, and the SACZ). Part II: Conditions of the circulations for generating the STCZs. *Journal of the Meteorological Society of Japan. Ser. II*, *71*(5), 581–610. https://doi.org/10.2151/jmsj1965.71.5_581

Koo, M.-S., & Hong, S.-Y. (2014). Stochastic representation of dynamic model tendency: Formulation and preliminary results. *Asia-Pacific Journal of Atmospheric Sciences*, *50*(4), 497–506.

Lau, K. M., Kim, M., & Kim, K. (2006). Asian summer monsoon anomalies induced by aerosol direct forcing: The role of the Tibetan Plateau. *Climate dynamics*, *26*(7-8), 855–864. https://doi.org/10.1007/s00382-006-0114-z

Lean, J., Rottman, G., Harder, J., & Kopp, G. (2005). SORCE contributions to new understanding of global change and solar variability. In *The Solar Radiation and Climate Experiment (SORCE)* (pp. 27–53). Springer. https://doi.org/10.1007/0-387-37625-9_3

Lee, J.-W., & Hong, S.-Y. (2014). Potential for added value to downscaled climate extremes over Korea by increased resolution of a regional climate model. *Theoretical and applied climatology*, *117*(3-4), 667–677.

Lee, J.-W., Hong, S.-Y., Chang, E.-C., Suh, M.-S., & Kang, H.-S. (2014). Assessment of future climate change over East Asia due to the RCP scenarios downscaled by GRIMs-RMP. *Climate dynamics*, *42*(3-4), 733–747. https://doi.org/10.1007/s00382-013-1841-6

Lee, J. W., Hong, S. Y., Kim, J. E. E., Yoshimura, K., Ham, S., & Joh, M. (2015). Development and implementation of river-routing process module in a regional climate model and its evaluation in Korean river basins. *Journal of Geophysical Research: Atmospheres*, *120*, 4613–4629. https://doi.org/10.1002/2014JD022698

Manzini, E., McFarlane, N., & McLandress, C. (1997). Impact of the Doppler spread parameterization on the simulation of the middle atmosphere circulation using the MA/ECHAM4 general circulation model. *Journal of Geophysical Research*, *102*(D22), 25,751–25,762. https://doi.org/10.1029/97JD01096

McPhaden, M. J., Zebiak, S. E., & Glantz, M. H. (2006). ENSO as an integrating concept in Earth science. *Science*, *314*(5806), 1740–1745. https://doi.org/10.1126/science.1132588

Meinshausen, M., Smith, S. J., Calvin, K., Daniel, J. S., Kainuma, M. L. T., Lamarque, J.-F., et al. (2011). The RCP greenhouse gas concentrations and their extensions from 1765 to 2300. *Climatic Change*, *109*(1-2), 213–241. https://doi.org/10.1007/s10584-011-0156-z

Mlawer, E. J., Taubman, S. J., Brown, P. D., Iacono, M. J., & Clough, S. A. (1997). Radiative transfer for inhomogeneous atmospheres: RRTM, a validated correlated-k model for the longwave. *Journal of Geophysical Research*, *102*(D14), 16,663–16,682. https://doi.org/10.1029/97JD00237

Morgenstern, O., Hegglin, M. I., Rozanov, E., O'Connor, F. M., Abraham, N. L., Akiyoshi, H., et al. (2017). Review of the global models used within phase 1 of the Chemistry-Climate Model Initiative (CCMI). *Geoscientific Model Development*, *10*(2), 639–671. http://doi.org/10.5194/gmd-10-639-2017

Murakami, T., & Matsumoto, J. (1994). Summer monsoon over the Asian continent and western North Pacific. *Journal of the Meteorological Society of Japan. Ser. II*, *72*(5), 719–745. https://doi.org/10.2151/jmsj1965.72.5_719

Newman, P. A., Nash, E. R., & Rosenfield, J. E. (2001). What controls the temperature of the Arctic stratosphere during the spring? *Journal of Geophysical Research*, *106*(D17), 19,999–20,010. https://doi.org/10.1029/2000JD000061

Ramanathan, V., Crutzen, P., Kiehl, J., & Rosenfeld, D. (2001). Aerosols, climate, and the hydrological cycle. *Science*, *294*(5549), 2119–2124. https://doi.org/10.1126/science.1064034

Rayner, N. (2003). Global analyses of sea surface temperature, sea ice, and night marine air temperature since the late nineteenth century. *Journal of Geophysical Research*, *108*(D14), 4407. https://doi.org/10.1029/2002JD002670

Riahi, K., Rao, S., Krey, V., Cho, C., Chirkov, V., Fischer, G., et al. (2011). RCP 8.5—A scenario of comparatively high greenhouse gas emissions. *Climatic Change*, *109*(1-2), 33–57. https://doi.org/10.1007/s10584-011-0149-y

Satheesh, S., & Ramanathan, V. (2000). Large differences in tropical aerosol forcing at the top of the atmosphere and Earth's surface. *Nature*, *405*(6782), 60. https://doi.org/10.1038/35011039

Stan, C., Straus, D. M., Frederiksen, J. S., Lin, H., Maloney, E. D., & Schumacher, C. (2017). Review of tropical-extratropical teleconnections on intraseasonal time scales. *Reviews of Geophysics.*, *55*, 902–937. https://doi.org/10.1002/2016RG000538

Trenberth, K. E., Branstator, G. W., Karoly, D., Kumar, A., Lau, N. C., & Ropelewski, C. (1998). Progress during TOGA in understanding and modeling global teleconnections associated with tropical sea surface temperatures. *Journal of Geophysical Research*, *103*(C7), 14,291–14,324. https://doi.org/10.1029/97JC01444

Wang, B., Wu, R., & Lau, K. (2001). Interannual variability of the Asian summer monsoon: Contrasts between the Indian and the western North Pacific–East Asian monsoons. *Journal of Climate*, *14*(20), 4073–4090. https://doi.org/10.1175/1520-0442(2001)014<4073:IVOTAS>2.0.CO;2

Xie, P., & Arkin, P. A. (1996). Analyses of global monthly precipitation using gauge observations, satellite estimates, and numerical model predictions. *Journal of Climate*, *9*(4), 840–858. https://doi.org/10.1175/1520-0442(1996)009<0840:AOGMPU>2.0.CO;2

Yeh, S.-W., Cai, W., Min, S.-K., McPhaden, M. J., Dommenget, D., Dewitte, B., et al. (2018). ENSO atmospheric teleconnections and their response to greenhouse gas forcing. *Reviews of Geophysics*, *56*, 185–206. https://doi.org/10.1002/2017RG000568

Yeh, S.-W., So, J., Lee, J.-W., Kim, M., Jeong, J., & Park, R. (2017). Contributions of Asian pollution and SST forcings on precipitation change in the North Pacific. *Atmospheric Research*, *192*, 30–37.

Zhao, S., Zhang, H., & Xie, B. (2018). The effects of El Niño–Southern Oscillation on the winter haze pollution of China. *Atmospheric Chemistry and Physics*, *18*(3), 1863.